

Fractal Prediction Model of Gas-Liquid Sulfur Phase Permeability Curve with Boundary Layer Considered

Jian-Yi Liu^{1*}, Lu Jiang¹, Miao Liu², Shan Yi³, Zhi-Bin Liu¹, Xue-Ni Dai¹, Yang Xie¹, Yi-Zhao Chen¹

1 State Key Laboratory of Oil and Gas Reservoir Geology and Exploitation, Southwest Petroleum University, No.8 Xindu Ave, Chengdu, 610500, China

2 Research Institute of Experimental and Detection, Petrochina Xinjiang Oilfield Company, Karamay, Xinjiang, 834000, China

3 Southwest Oil and Gas Field Company, Petro-China, Chengdu, People's Republic of China.

ABSTRACT

The liquid sulfur precipitated from high-sulfur gas reservoir will change the situation of only single-phase gas permeability. Moreover, the continuous accumulation of precipitated liquid sulfur will bring certain damages to the reservoir, reduce the productivity and affect the development of gas well. In order to define the law of gas-liquid sulfur phase permeability, this paper sets up a flow resistance model considering the liquid sulfur boundary layer at the pore scale including the capillary force, gas phase viscosity force and liquid sulfur phase viscosity force. Then in combination with the fractal theory of porous media, this paper establishes the prediction model of gas-liquid sulfur relative permeability and compares the prediction curve calculated by the model with the result of real core gas-liquid sulfur phase permeability experiment in non-steady state. According to the comparison result, the mathematical model of gas-liquid sulfur phase permeability can reflect the features of gas-liquid sulfur phase permeability, but there is a certain error with the experimental results, for instance, the sulfur saturation of isotonic point is 5% less than the experimental result while the relative permeability of isotonic point is 10% higher than the experimental result. This is because the mathematical model of phase permeability is deduced based on the steady state theory while in the experiment the non-steady state method is adopted. The two methods are based on different assumptions, which naturally results in a certain error.

Keywords: flow resistance, gas-liquid sulfur phase permeability, liquid sulfur adsorption boundary layer

NONMENCLATURE

Symbols

A	Fractal area of porous media, m ²
D_f	Core fractal dimension
D_T	Tortuosity fractal dimension
h	Capillary number in core, dimensionless
l_δ	Distance required to form a stable boundary layer, m
l_g	Length of gas section, m
P_{c1}	Capillary pressure at right end of gas phase in distribution form 1, Pa
P_{vs1r}	Sulfur viscosity of throat liquid in distribution 1, Pa
P_{vs2}	Total liquid sulfur viscosity of Distribution 2, Pa
ΔP	Pressure difference between two ends of capillary, Pa
Q_g	Gas flow in core, m ³ /s
Q_s	Liquid sulfur flow in core, m ³ /s
R	Throat radius, m
r	Capillary radius, m
S_{sr}	Bound sulfur saturation, %
S_{gr}	Residual gas saturation, %
θ	Gas phase wetting angle, °
τ_g	Gas phase tortuosity, decimal
τ_s	Tortuosity of liquid sulfur phase, decimal
ρ_s	Density of liquid sulfur, kg/m ³
δ	Boundary layer thickness, m

λ_{\max}	Maximum capillary diameter,m
v	Fluid velocity,m/s

1. INTRODUCTION

Relative permeability, which is used as a quantitative parameter to describe the flow law of multiphase fluid in porous media, has been widely applied in multiple fields including the petroleum engineering and soil science. The methods of testing phase permeability curve can be divided into two situations: the steady state and non-steady state. The former refers to the method of establishing stable two-phase core flow conditions in different fluid ratios to calculate the relative permeability of each phase according to the Darcy Law; the latter refers to the method of establishing the two-phase flow in the core in different saturations by displacement to calculate the permeability of each phase under different water saturations in the core.

In the reservoir layer, the liquid sulfur can be dissolved in acid gas in physical/chemical reaction. When the sulfur content in the gas reaches supersaturation, the elemental sulfur will be gradually precipitated^{[1][2][3]}. At different temperature levels, the sulfur precipitated from acid gas reservoir can stay in the state of liquid and solid respectively, which will both affect the gas flow in porous media.

In the experiment, the solid sulfur can only be converted from solid to liquid at 385.95K, so it's hard to obtain the gas-liquid sulfur phase permeability curve in the non-steady state. Moreover, it's very hard to control the gas-liquid sulfur injection ratio in high temperature, so it's almost impossible to conduct the experiment of phase permeability in the steady state. It's hard for use to find any current researches on the experiment of gas-liquid sulfur phase permeability. Therefore, we need to establish a theoretical prediction model for the gas-liquid sulfur phase permeability curve to reveal the relevant mechanism.

The theory-based methods of calculating the permeability curve can be divided into two kinds: the calculation based on capillary force^{[5][6]} and the power function empirical formula^{[7][8]}. Both methods can effectively predict the permeability curve. However, in high-sulfur gas reservoir, the boundary layer generated on the wall during liquid sulfur flow will affect the displacement mechanism of gas and liquid sulfur, so the influence of boundary layer shall be taken into consideration when establishing the model to predict the gas-liquid sulfur phase permeability curve.

Based on the method of calculating permeability by capillary force curve, we introduce the influence of boundary layer generated by the precipitated sulfur on the gas-liquid sulfur two-phase permeability, establish the porous medium gas-liquid sulfur two-phase pore-throat displacement mechanism and set up the prediction model of gas-liquid sulfur phase permeability curve by fractal theory to characterize the core heterogeneity.

2. MODEL OF GAS-LIQUID SULFUR TWO-PHASE FLOW RESISTANCE

When studying the gas-liquid sulfur two-phase flow mechanism, it's necessary to discuss the two-phase flow resistance at the pore scale first. In this summary, we consider the pore-throat unit as the physical model and deduce a gas-liquid sulfur two-phase flow resistance model considering the thickness of liquid sulfur boundary layer to be used as the basis for the subsequent mathematical model of gas-liquid sulfur phase permeability.

2.1 Gas-Liquid Sulfur Two-Phase Distribution Pore-Throat Model

The pore space of the core is simplified into a series of parallel capillaries, each of which is connected by n pore-throat units. When it's assumed that the pore-throat unit is fully saturated with liquid sulfur, the gas will conduct piston displacement on the liquid sulfur in the pore-throat unit from left to right. The distribution of liquid sulfur boundary layer is shown in Fig. 2-1

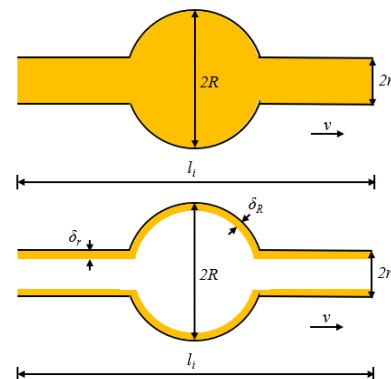


Fig. 2-1 Schematic diagram of liquid sulfur boundary layer in pore throat unit

2.2 Introduction Model of Liquid Sulfur Boundary Layer Thickness

When deducing the mathematical model of liquid sulfur boundary layer thickness, the following assumptions shall be made:

- (1) Liquid sulfur and gas flow in the capillary layer;

(2) During the flow of liquid sulfur and gas, only liquid sulfur will produce a boundary layer, which is symmetrically and evenly distributed inside the capillary wall, as shown in Fig. 2-1.

(3) All fluids are incompressible.

Based on the von Karman boundary layer integral equation of steady incompressible fluid flow, the pressure derivative at the wall is 0:

$$\rho_s \frac{\partial}{\partial x} \left(\int_0^\delta v_{(x)}^2 dy \right) - \rho_s v \frac{\partial}{\partial x} \left(\int_0^\delta v_{(x)} dy \right) = -\tau_s \quad (2-1)$$

It is assumed that the velocity distribution in the liquid sulfur boundary layer can be approximately expressed as:

$$v_{(x)} = a_0 + a_1 y + a_2 y^2 + a_3 y^3 + a_4 y^4 \quad (2-2)$$

Combined with the boundary conditions, the approximate expression of velocity distribution in the liquid sulfur boundary layer is obtained as follows:

$$v_{(x)} = 2 \frac{v}{\delta} y - 2 \frac{v}{\delta^3} y^3 + \frac{v}{\delta^4} y^4 \quad (2-3)$$

Combined with formula 2-1 and 2-3, the shear stress τ_s generated by liquid sulfur and the wall surface is expressed as follows:

$$\tau_s = \mu_s \left(\frac{dv}{dy} \right)_{y=0} = \frac{2\mu_s v}{\delta} \quad (2-4)$$

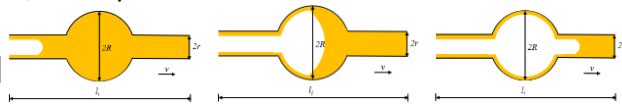
The thickness of boundary layer considering liquid sulfur precipitation is as follows:

$$\delta = 5.83 \sqrt{\frac{\mu_s l_s}{\rho_s v}} \quad (2-5)$$

The thickness of liquid sulfur boundary layer at different liquid sulfur flow rates can be calculated by the above formula.

2.3 Fluid Distribution in Pore-Throat Unit

Based on the pore throat distribution model in the upper section, it is concluded that there are three types of gas-liquid sulfur distribution in the process of gas drive sulfur, namely:



(a) Distribution form 1 (b) Distribution form 2 (c) Distribution form 3

Fig. 2-2 Schematic diagram of gas drive liquid sulfur

In the distribution form 1, the gas is displaced into the left throat of the pore-throat unit, but has not yet access to the middle pore. The force received is mainly the capillary force generated when the gas displaces the liquid sulfur, the gas phase viscosity force when the gas flows into the throat and the liquid phase viscosity force

generated when the remaining liquid sulfur flows in the pore-throat unit. At this moment, the gas viscosity force is small while the fluid viscosity force is large. When the gas is displaced into the intermediate pores as shown in the distribution pattern 2, the capillary force still exists then and the gas phase viscosity force will gradually increase in the process of displacement while the liquid phase viscosity force will gradually decrease; in the distribution form 3, the gas is displaced into the right throat of the pore-throat unit. The liquid phase viscosity force will gradually disappear while the gas phase viscosity force will increase to the maximum level.

2.4 Model of Flow Resistance

Based on the pore-throat unit model, the coordinate system is established to analyze the gas-liquid sulfur two-phase flow resistance. According to the location of gas-liquid sulfur interface, there are three situations as follows: interface in left throat, interface in intermediate pore and interface in right throat. Therefore, the abscissas of points A and B in Figure 2-3 shall be determined to make the classification and analyze the gas-phase flow resistance, capillary force and liquid-phase flow resistance in each of the aforesaid situations.

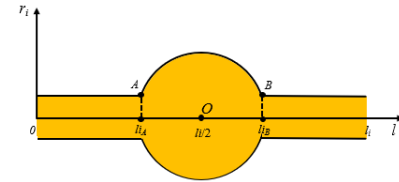


Fig. 2-3 Analysis of flow resistance of orifice throat unit and establishment of coordinate system

(1) flow resistance model of distribution form 1

When $0 \leq l_{gi} < [l_i/2 - (R^2 - r^2)^{1/2}]$, The flow resistance of orifice throat unit is shown in Fig. 2-4.

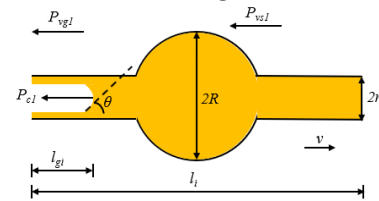


Fig. 2-4 Flow resistance diagram of distribution form 1

In distribution 1, the pressure difference at both ends of capillary is the sum of gas flow resistance and liquid sulfur flow resistance (i.e. liquid sulfur viscous force).

$$\Delta P_1 = P_{vsl} + \Delta P_{g1} = \frac{8\mu_s v}{r^2} \left[l_i - 2(R^2 - r^2)^{1/2} - l_{gi} \right] + \int_0^{l_{gi}} \frac{l_{gi} + (R^2 - r^2)^{1/2}}{2(R^2 - r^2)^{1/2}} \frac{8\mu_s v}{R^2 - (l_{gi} - l_i/2)^2} \cdot dl_{gi} + \frac{2\sigma \cos \theta}{r - \delta_r} + \frac{8\mu_g v}{(r - \delta_r)^2} \cdot l_{gi} \quad (2-6)$$

(2) flow resistance model of distribution form 2

When $[l_i/2 - (R^2 - r^2)^{1/2}] \leq l_{gi} < [l_i/2 + (R^2 - r^2)^{1/2}]$, The flow resistance of orifice-throat unit is shown in Fig. 2-5.

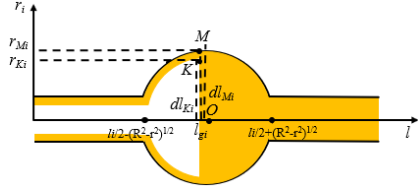


Fig. 2-5 Flow resistance diagram of distribution form 2

The resistance of gas-liquid-sulfur two-phase flow ΔP_2 is equal to the sum of liquid-phase flow resistance and gas-phase flow resistance ΔP_{g2} . The resistance of liquid phase flow is the viscosity of liquid sulfur P_{vs2} .

$$\begin{aligned} \Delta P_2 &= P_{vs2} + \Delta P_{g2} \\ &= \frac{2\sigma \cos \theta}{\sqrt{(R - \delta_r)^2 - (l_{gi} - l_i/2)^2}} + \frac{8\mu_g v}{(r - \delta_r)^2} \cdot \left[\frac{l_i}{2} - (R^2 - r^2)^{1/2} \right] \\ &\quad + \int_{\frac{l_i}{2} - (R^2 - r^2)^{1/2}}^{l_{gi}} \frac{8\mu_g v}{(R - \delta_r)^2 - (l_{gi} - l_i/2)^2} dl_{gi} \\ &\quad + \int_{l_{gi}}^{\frac{l_i}{2} + (R^2 - r^2)^{1/2}} \frac{8\mu_g v}{R^2 - (l_{gi} - l_i/2)^2} dl_{gi} + \frac{8\mu_g v}{r^2} \cdot \left[\frac{l_i}{2} - (R^2 - r^2)^{1/2} \right] \end{aligned} \quad (2-7)$$

(3) flow resistance model of distribution form 3

When $[l_i/2 + (R^2 - r^2)^{1/2}] \leq l_{gi} \leq l_i$, The flow resistance of orifice throat unit is shown in Fig. 2-6.

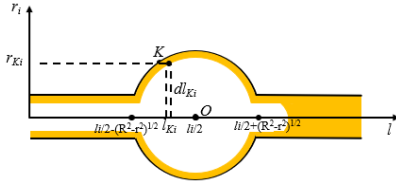


Fig. 2-6 Flow resistance diagram of distribution form 3

The total gas-liquid sulfur two-phase flow resistance ΔP_3 is equal to the sum of liquid-phase flow resistance (i.e. liquid sulfur viscous force P_{vs3}) and gas-phase flow resistance ΔP_{g3} .

$$\begin{aligned} \Delta P_3 &= P_{vs3} + \Delta P_{g3} \\ &= \frac{8\mu_g v}{r^2} (l_i - l_{gi}) + \int_{l_i/2 - (R^2 - r^2)^{1/2}}^{l_i/2 + (R^2 - r^2)^{1/2}} \frac{8\mu_g v}{(R - \delta_r)^2 - (l_{ki} - l_i/2)^2} dl_{ki} \\ &\quad + \frac{8\mu_g v}{(r - \delta_r)^2} \cdot \left[l_i - 2(R^2 - r^2)^{1/2} \right] + \frac{2\sigma \cos \theta}{r - \delta_r} \end{aligned} \quad (2-8)$$

By using the core parameters of target block, the flow resistance is transformed into the relationship between sulfur saturation, and determine reasonable pore throat combination and flow rate, and then combined with the mathematical model of gas-liquid sulfur infiltration, the calculation is carried out.

3. FRACTAL PHASE PERMEATION MODEL OF GAS LIQUID SULFUR

The fractal permeability of porous media can be expressed as^[4]:

$$K = \frac{\pi}{128} \frac{L_0^{1-D_f}}{A} \frac{D_f}{3+D_f-D_f} \lambda_{\max}^{3+D_f} \quad (3-1)$$

The fractal flow rate of porous media can be expressed as^[4]:

$$Q = \frac{\pi \Delta P}{128 L_0^{D_f} \mu} \frac{D_f}{3+D_f-D_f} \lambda_{\max}^{3+D_f} \quad (3-2)$$

Assuming that there are h capillaries in the core, the gas flow rate Q_{gh} and the liquid sulfur flow rate in the core are Q_s :

$$Q_g = \sum q_g = \sum_{j=1}^h \frac{n^{D_f} \pi (P_{vgj} + P_{cj})}{128 (1-S_s)^{D_f} (\lambda^{1-D_f} \square L_0^{D_f})^{D_f} \mu_g} \frac{D_f}{3+D_f-D_f} (2r_{eq-g})^{3+D_f} \quad (3-3)$$

$$Q_s = \sum q_s = \sum_{j=1}^h \frac{n^{D_f} \pi}{128 (\lambda^{1-D_f} \square L_0^{D_f})^{D_f} \mu_s} \frac{D_f}{3+D_f-D_f} \left[\Delta P_l (2r_{eq-l})^{3+D_f} - \frac{P_{vgj} + P_{cj}}{(1-S_s)^{D_f}} (2r_{eq-g})^{3+D_f} \right] \quad (3-4)$$

According to the tortuosity formula of gas phase and liquid phase, considering the irreducible sulfur saturation (S_{sr}) and residual gas saturation (S_{gr}) in the core, the following results are obtained:

$$\begin{aligned} k_{rg} &= \tau_g^2 \frac{\int_{S_s}^{1-S_{gr}} \frac{P_{vgj} + P_{cj}}{P_c^{2(3+D_f)}} (1-S_s)^{\frac{3}{4}(1-D_f)} d(S_s)^{\frac{3+D_f}{4}}}{\int_0^1 \frac{\Delta P_l}{P_c^{2(3+D_f)}} d(S_s)^{\frac{3+D_f}{4}}} \\ k_{rs} &= \tau_s^2 \frac{\int_{S_{sr}}^{1-S_{gr}} \frac{\Delta P_l}{P_c^{2(3+D_f)}} d(S_s)^{\frac{3+D_f}{4}} - \int_{S_s}^{1-S_{gr}} \frac{P_{vgj} + P_{cj}}{P_c^{2(3+D_f)}} (1-S_s)^{\frac{3}{4}(1-D_f)} d(S_s)^{\frac{3+D_f}{4}}}{\int_0^1 \frac{\Delta P_l}{P_c^{2(3+D_f)}} d(S_s)^{\frac{3+D_f}{4}}} \end{aligned} \quad (3-5)$$

$$\tau_g = \frac{1-S_s - S_{gr}}{1-S_{sr} - S_{gr}}, \quad \tau_s = \frac{S_s - S_{sr}}{1-S_{sr}}$$

The formula above is the gas-liquid sulfur fractal permeability model established in this paper, which considers the influence of boundary layer generated during sulfur deposition and reflects the heterogeneity feature of the core. Substituting into the model the relationship between flow resistance and saturation level established in Chapter 2, we can predict the gas-liquid sulfur phase permeability curve of the core.

4. EXPERIMENTAL RESULTS AND COMPARATIVE ANALYSIS

The unsteady phase permeability experiment was carried out with the core of a high sulfur gas reservoir, and the core related parameters were tested as follows: Table 5-1 basic core parameters for gas liquid sulfur unsteady phase permeability experiment

number	length (mm)	diameter (mm)	weight (g)	Φ (%)	K (mD)
22	49.40	25.16	58.8624	15.01	103.70

The capillary force curve converted from nuclear magnetic resonance data is used in the calculation of gas-liquid sulfur infiltration mathematical model. The

experimental data of core 22 are compared with the model results, as shown in Fig. 4-1.

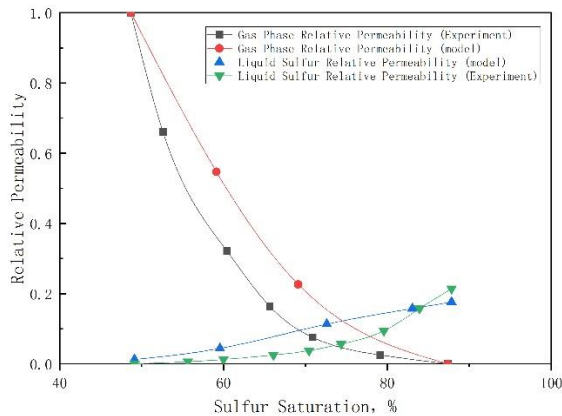


Fig. 4-1 Comparison between experimental data and mathematical model

According to the Figure 4-1, it can be seen that the gas phase permeability curve and the liquid sulfur phase permeability curve are not highly coincident if we only focus on the comparison between the experimental data of No. 22 core and the mathematical model. There is a certain error with the prediction results, for instance, the sulfur saturation of isotonic point is 5% less than the experimental result and the relative permeability of isotonic point is 10% higher than the experimental result. This is because the mathematical model of phase permeability is deduced based on the steady state theory while the experiment is done based on the non-steady state method. The two methods are based on different assumptions, which naturally results in a certain error.

5. CONCLUSION

(1) The model of liquid sulfur displacement boundary layer is established based on the Von Karman boundary layer integral equation for the steady flow of incompressible fluid to calculate the boundary layer thickness at different liquid sulfur speeds.

(2) According to different displacement positions of gas-liquid sulfur phase in the pore-throat unit, three types of gas-liquid sulfur distribution in the core are obtained with corresponding gas-liquid sulfur two-phase flow resistance model. The flow resistance is converted into the relationship with the sulfur saturation by relevant parameters, so that the specific data can be substituted into the mathematical model of gas-liquid sulfur phase permeability for calculation.

(3) Establish the gas-liquid sulfur fractal permeability model considering the sulfur deposition boundary layer, assume different pore-throat combinations and predict

the core permeability curve by means of capillary pressure curve.

(4) Because the gas-liquid sulfur phase permeability curve in stable state cannot be obtained in laboratory, we compare the prediction results of this model with the gas-liquid sulfur phase permeability curve in non-stable state and find there's a certain error, e.g. the sulfur saturation of isotonic point is 5% less than the experimental result and the relative permeability of isotonic point is 10% higher than the experimental result.

ACKNOWLEDGEMENT

This work was supported by the National Science and Technology Major Project (Grant No. 2016ZX05053).

REFERENCE

- [1]C.-Y Sun,G.-J Chen. Experimental and modeling studies on sulfur solubility in sour gas[J]. Fluid Phase Equilibria,2003,214(2).
- [2]Roberts B E.The Effect of Sulfur Deposition on Gaswell Inflow Performance[J]. Spe Reservoir Engineering, 1997,12(2):118-123.
- [3]Gu Min-Xin,Li Qun,Zhou Shan-Yan,Chen Wei-Dong,Guo Tian-Min. Experimental and modeling studies on the phase behavior of high H₂S-content natural gas mixturesag[J]. Elsevier,1993,82.
- [4]Boming Yu, Ping Cheng. A fractal permeability model for bi-dispersed porous media[J]. International Journal of Heat & Mass Transfer, 2002, 45(14):2983-2993.
- [5]Burdine N T . Relative Permeability Calculations From Pore Size Distribution Data[J]. Petr.trans.am Inst.mining Metall.eng, 1953, 98(3):71-78.
- [6]Mualem, Yechezkel. A new model for predicting the hydraulic conductivity of unsaturated porous media[J]. Water Resources Research, 1976, 12(3):513-522.
- [7]Cary J W , Simmons C S , McBride J F . Predicting Oil Infiltration and Redistribution in Unsaturated Soils[J]. Soil ence Society of America Journal, 1989, 53(2):335-342.
- [8]Wyllie, M. R. J., Relative permeability, in Petroleum Production Handbook, vol. II, Reservoir Engineering, edited by T. C. Frick and R. W. Taylor, pp. 25.1-25.14, McGraw-Hill, New York, 1962.